

Novel Diethyl Ether Gas Sensor Based on Cataluminescence on Nano-Pd/ZnNi₃Al₂O₇

Wenjuan Zhang, Fuxiu Yang, Baining Liu,* and Kaowen Zhou*

Cite This: *ACS Omega* 2021, 6, 17576–17583

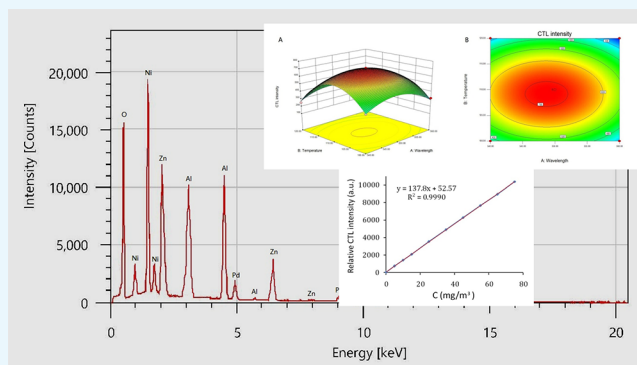
Read Online

ACCESS |

Metrics & More

Article Recommendations

ABSTRACT: A sensitive diethyl ether gas sensor based on cataluminescence on nano-Pd/ZnNi₃Al₂O₇ at a temperature lower than 150 °C was reported. The composition of the sensitive material was determined by energy-dispersive spectrometry, and a particle size of less than 50 nm was shown by transmission electron microscopy. When the atomic percentage of Pd in the sensing material is 0.8–1.3%, it is beneficial to the low-temperature and high-selective cataluminescence of diethyl ether. The signal response and recovery of diethyl ether on the sensitive material can be completed quickly in 0.5 s, and the relative standard deviation of the signal within 500 h of continuous operation is not more than 2.5%. There is good linear relationship between the luminescence intensity and the concentration of diethyl ether in the range of 0.08–75 mg/m³. The detection limit (3σ) is 0.04 mg/m³. The working conditions optimized by the response surface methodology were an analytical wavelength of 548.86 nm, a reaction temperature of 109.18 °C, and a carrier gas velocity of 125.88 mL/min. The sensitivity of the method can be increased by 4.5% under the optimized working conditions. The optimization method is universal for many multi-parameter processes.



INTRODUCTION

Diethyl ether is a colorless and flammable liquid, which is very volatile and can be miscible with ethanol, acetone, benzene, and chloroform. The mixture of gaseous diethyl ether and 10 times volume of oxygen can explode violently in the case of fire or electric spark.^{1,2} Diethyl ether in air not only has safety problems but also affects human health. A large concentration of diethyl ether may cause the person in contact with it to be excited, then be sleepy, vomit, be pale, and have a slow pulse, hypothermia, and irregular breath, even life-threatening. Most of the fatal cases involving diethyl ether reported in the second half of the 19th century and the first half of the 20th century were related to anesthesia as diethyl ether was widely used as an anesthetic in many countries during this period.³ When people inhale low-concentration diethyl ether for a long time, they may have headache, dizziness, tiredness, drowsiness, proteinuria, and erythrocytosis. Therefore, it is necessary to determine the content of diethyl ether in air simply and quickly.

Diethyl ether in air is usually determined by gas chromatography with direct injection. Because this method requires a gas chromatograph, it cannot be done on the spot. Gas sensors are especially suitable for on-site, online, or remote measurements. Up to now, there are few reports about other sensing technologies of diethyl ether besides cataluminescence (CTL). CTL, a kind of chemiluminescence (CL) emitted from

heterogeneous catalytic oxidation reactions on the gas–solid interface, has been considered as a promising energy transduction mechanism for fabricating gas sensors.⁴ In recent years, a series of CTL sensing applications have been attempted to develop for diethyl ether^{5–14} and many other molecules^{15–35} at different laboratories. However, a higher working temperature above 200 °C is not conducive to the stability of the sensor signal.⁴

Metal oxides and their doped composites have been widely used in many catalytic reaction-related fields due to their excellent heterogeneous catalytic performance, low cost, stability, and easy availability.^{36–41} Pd-doped composites often exhibit low-temperature catalytic oxidation activities for many molecules.^{42–46} Our team has found that Pd/ZnNi₃Al₂O₇ has low-temperature CTL activity for diethyl ether.⁴⁷ It may be a good attempt to fabricate gas sensors by using Pd/ZnNi₃Al₂O₇ as a sensitive material.

Received: April 20, 2021

Accepted: June 15, 2021

Published: June 29, 2021



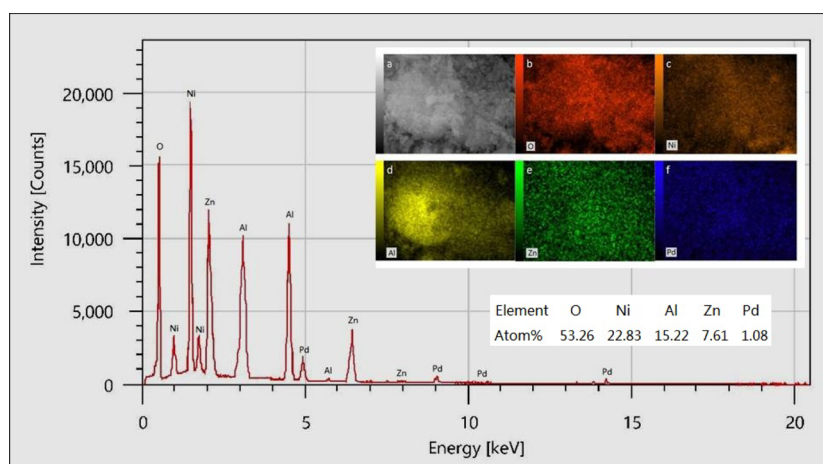


Figure 1. EDS spectrum of the sensitive material. (a) SEM image of the test area, (b) element mapping of oxygen, (c) element mapping of nickel, (d) element mapping of aluminum, (e) element mapping of zinc, and (f) element mapping of palladium.

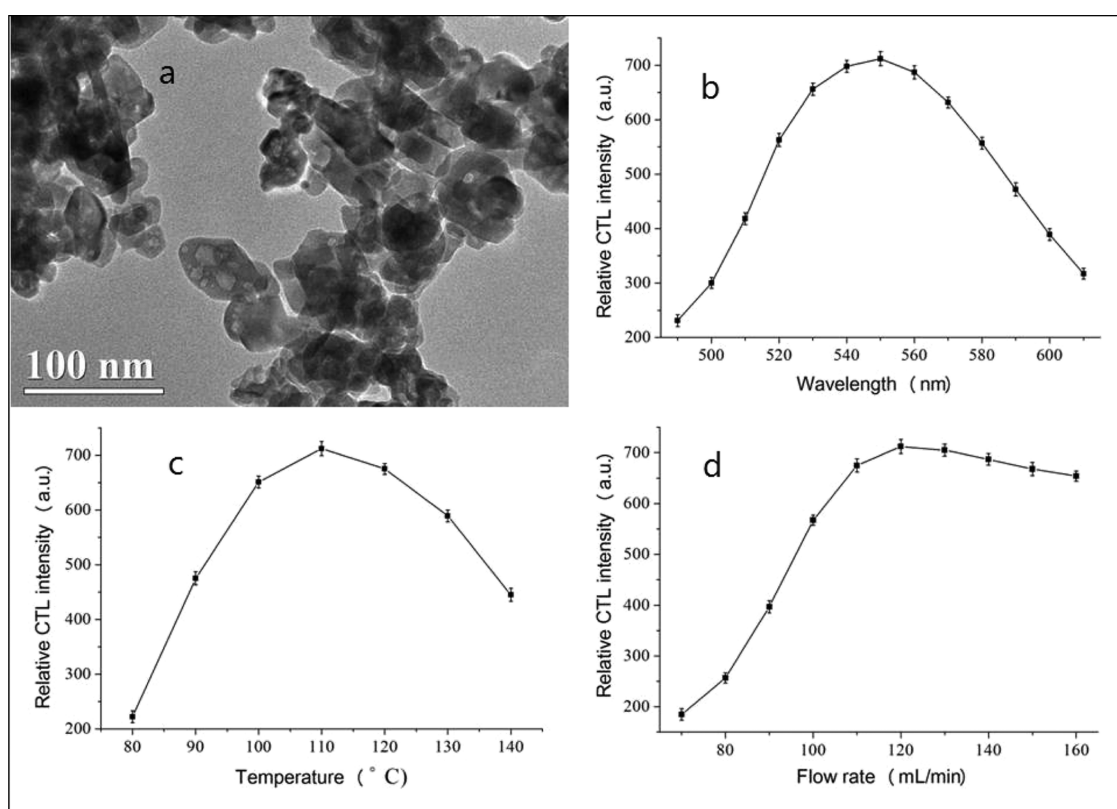


Figure 2. (a) TEM image of the sensitive material, (b) CTL spectrum of diethyl ether, (c) temperature dependence of the CTL intensity of diethyl ether, and (d) carrier gas velocity dependence of the CTL intensity of diethyl ether.

The main working conditions for the determination of diethyl ether by the CTL method, such as analytical wavelength, working temperature, and carrier gas flow rate, are not isolated but interact with each other. The response surface method (RSM) is a statistical comprehensive test technique.^{32–35,48–51} It takes the response of the system as a function of many factors and displays the functional relationship by the graphic technology. In this way, we can choose the optimal conditions in the experimental design by intuitive observation. In this work, first, Pt-doped $\text{ZnNi}_3\text{Al}_2\text{O}_7$ was synthesized and characterized. Then, the experimental conditions were optimized by RSM, and the low-temperature

CTL properties of the composite were studied. Finally, a feasible method was established for determining diethyl ether by utilizing CTL at a temperature lower than 150 °C.

RESULTS AND DISCUSSION

Characterization of Sensitive Materials. The energy-dispersive spectrometry (EDS) spectrum in Figure 1 shows that the prepared sensitive material is 100% $\text{Pd}/\text{ZnNi}_3\text{Al}_2\text{O}_7$ because the atomic ratio of O, Ni, Al, and Zn is close to 7:3:2:1. It is found that the content of the Pd atom in sensitive materials has a great influence on their CTL activity. When the atomic percentage of Pd is less than 0.8%, the sensitive

material has CTL activity to diethyl ether only when the temperature is above 200 °C. When the atomic percentage of Pd is more than 1.3%, in addition to diethyl ether, formaldehyde, acetaldehyde, sulfur dioxide, hydrogen sulfide, and ammonia also have obvious CTL signals.

The element mapping in the illustration of Figure 1 shows that oxygen, nickel, aluminum, zinc, and palladium were uniformly distributed in the prepared sensitive material. The transmission electron microscopy (TEM) image in Figure 2a shows that the size of Pd/ZnNi₃Al₂O₇ is not more than 50 nm.

Choice of Experimental Conditions by the Single-Factor Test. In this part, the effects of analysis wavelength, reaction temperature, and carrier gas velocity on the CTL intensity of 5 mg/m³ diethyl ether on sensitive materials were separately studied. Figure 2b is a CTL spectrum of diethyl ether on nano-Pd/ZnNi₃Al₂O₇ at 110 °C with a carrier gas velocity of 120 mL/min. The CTL intensities were high at 550 nm. Figure 2c shows the temperature dependence of the CTL intensity of diethyl ether at a wavelength of 550 nm under a carrier gas velocity of 120 mL/min. As can be seen, the temperature of around 110 °C will be favorable to the determination of diethyl ether. Figure 2d shows the carrier gas velocity dependence of the CTL intensity of diethyl ether at 550 nm and 110 °C. The CTL intensity increased with an increase in the carrier gas velocity below 120 mL/min, and it decreased above this velocity.

It can be seen that the operating conditions of simple optimization through single-factor experiments are an analysis wavelength of 550 nm, a working temperature of 110 °C, and a carrier gas velocity 120 mL/min.

Optimization of Experimental Conditions by RSM. Now, we take CTL intensity as a function of three experimental conditions. The effects of analysis wavelength, reaction temperature, and carrier gas velocity on CTL intensity were studied by RSM. Table 1 is a three-factor and three-level Box–Behnken test set according to the test conditions selected by the single factor.

Table 1. Factors and Levels of the Box–Behnken Test Design

| factors levels | wavelength (nm) | temperature (°C) | flow rate (mL/min) |
|----------------|-----------------|------------------|--------------------|
| −1 | 540 | 100 | 110 |
| 0 | 550 | 110 | 120 |
| 1 | 560 | 120 | 130 |

The results of 17 response surface design trials (12 edge points plus 5 center points in Box–Behnken test design) for 5 mg/m³ diethyl ether are shown in Table 2.

The 3D surfaces and contours are plotted by Design Expert software, as shown from Figures 3–5. Each figure represents the interaction of two independent variables on the CL intensity.

Figure 3 shows the 3D surface (A) and contours (B) of the effects of analysis wavelength and reaction temperature on the CTL intensity, respectively. With the increase of the analysis wavelength and reaction temperature, the CTL intensity increases. When the analysis wavelength reaches 548.86 nm and the reaction temperature reaches 109.18 °C, the CTL intensity reaches its maximum. When the analysis wavelength and reaction temperature continue to increase, the CTL intensity begins to decrease.

Table 2. Response Surface Design Arrangement and Experimental Results

| number | wavelength (nm) | temperature (°C) | flow rate (mL/min) | CL intensity (a.u.) |
|--------|-----------------|------------------|--------------------|---------------------|
| 1 | 540.00 | 120.00 | 120.00 | 251 |
| 2 | 550.00 | 100.00 | 110.00 | 311 |
| 3 | 540.00 | 110.00 | 110.00 | 437 |
| 4 | 560.00 | 110.00 | 130.00 | 547 |
| 5 | 550.00 | 110.00 | 120.00 | 712 |
| 6 | 540.00 | 100.00 | 120.00 | 362 |
| 7 | 550.00 | 110.00 | 120.00 | 711 |
| 8 | 550.00 | 110.00 | 120.00 | 713 |
| 9 | 560.00 | 100.00 | 120.00 | 309 |
| 10 | 540.00 | 110.00 | 130.00 | 635 |
| 11 | 550.00 | 120.00 | 130.00 | 394 |
| 12 | 550.00 | 110.00 | 120.00 | 711 |
| 13 | 560.00 | 120.00 | 120.00 | 195 |
| 14 | 550.00 | 120.00 | 110.00 | 237 |
| 15 | 550.00 | 110.00 | 120.00 | 713 |
| 16 | 560.00 | 110.00 | 110.00 | 308 |
| 17 | 550.00 | 100.00 | 130.00 | 467 |

Figure 4 shows the 3D surface (A) and contours (B) of the effects of analysis wavelength and carrier gas velocity on the CTL intensity, respectively. As can be seen, when the analytical wavelength reaches 548.86 nm and the carrier gas velocity reaches 125.88 mL/min, the CTL intensity reaches its maximum.

Figure 5 shows the 3D surface (A) and contours (B) of the effects of reaction temperature and carrier gas velocity on the CTL intensity, respectively. As can be seen, when the reaction temperature reaches 109.18 °C and the carrier gas velocity reaches 125.88 mL/min, the CTL intensity reaches its maximum.

Based on the above experimental results, it can be found that the optimum values of analysis wavelength, reaction temperature, and carrier gas velocity are 548.86 nm, 109.18 °C, and 125.88 mL/min, respectively, when the maximum CTL intensity is obtained. It is almost impossible to obtain the optimal operating conditions through single-factor experiments because the number of experiments needed is very large. According to the model, the maximum value of CTL intensity was 744. This is 4.5% higher than the CTL intensity under single-factor optimization conditions, which will correspondingly improve the sensitivity of the method.

Sensing Properties. To investigate the lifetime of the sensitive materials, an experiment was carried out by continually introducing 20 mg/m³ diethyl ether in air with the velocity of 125.88 mL/min to the surface of sensitive materials at 109.18 °C and detecting the CTL intensities once every hour at 548.86 nm. Partially recording signals are shown in Figure 6A. The results showed that the relative standard deviation (RSD) of CTL intensities was less than 2.5% for continuous 500 h detection. Further experiments showed that the RSD of the CTL intensities was within 5% for daily use above 10 months. It can be said that nano-Pd/ZnNi₃Al₂O₇ has a long service life for diethyl ether monitoring.

Fast signal response is one of the important indicators of sensors. Response characteristics of CTL signals for diethyl ether under the optimization conditions were investigated. Figure 6B signifies that both the response and recovery of diethyl ether are within 0.5 s.

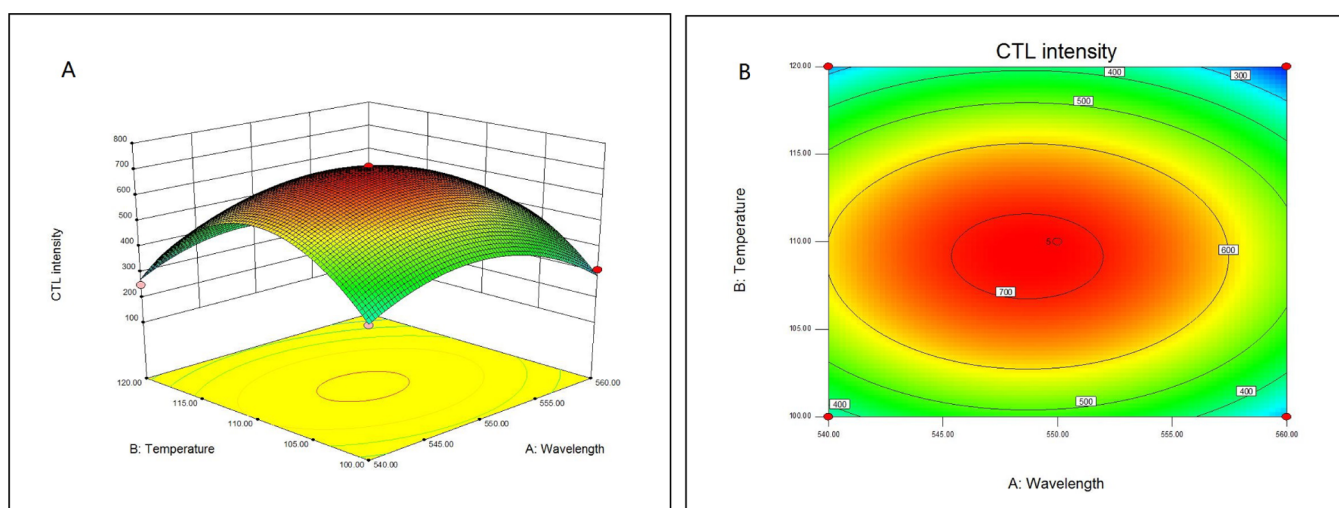


Figure 3. Response surface (A) and contours (B) of the interaction of analysis wavelength and reaction temperature on the CTL intensity.

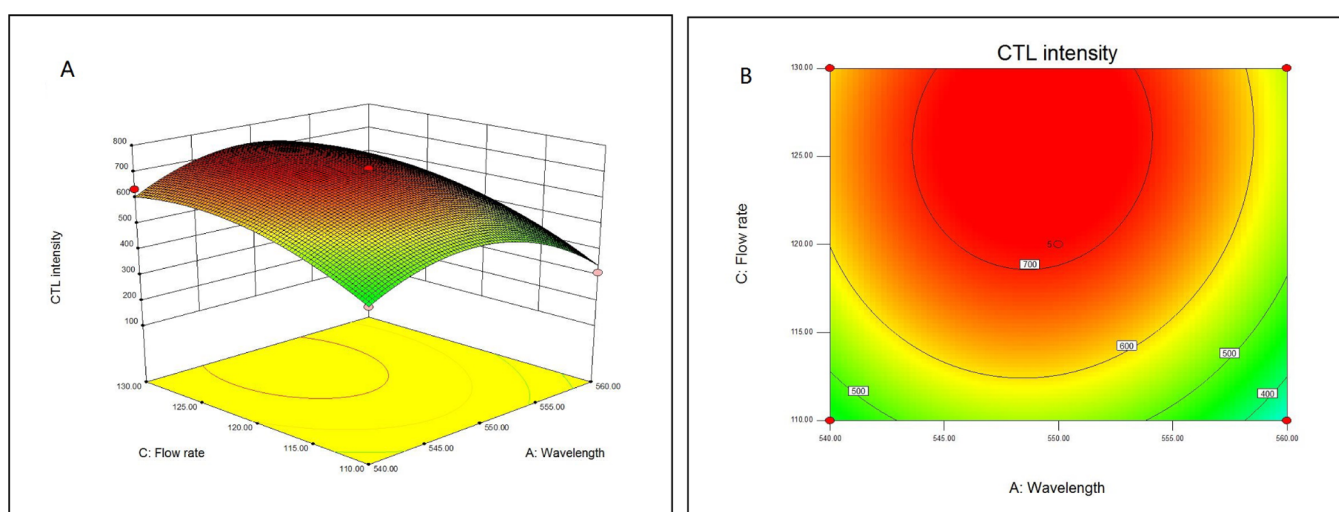


Figure 4. Response surface (A) and contours (B) of the interaction of analysis wavelength and carrier gas velocity on the CTL intensity.

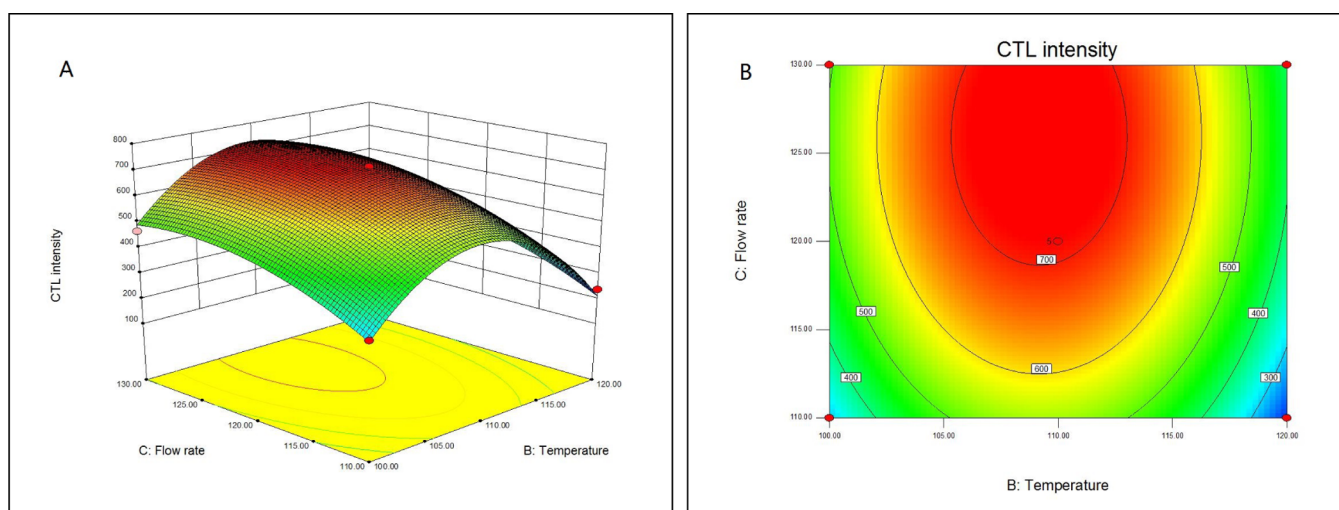


Figure 5. Response surface (A) and contours (B) of the interaction of reaction temperature and carrier gas velocity on the CTL intensity.

The CTL signals from diethyl ether were much larger than those from other molecules. The signals from formaldehyde, formic acid, acetic acid, carbon monoxide, and methyl ether

were less than 2% of diethyl ether. No visible signals were obtained from methanol, ethanol, acetaldehyde, benzene, hydrogen sulfide, and sulfur dioxide. It indicated that nano-

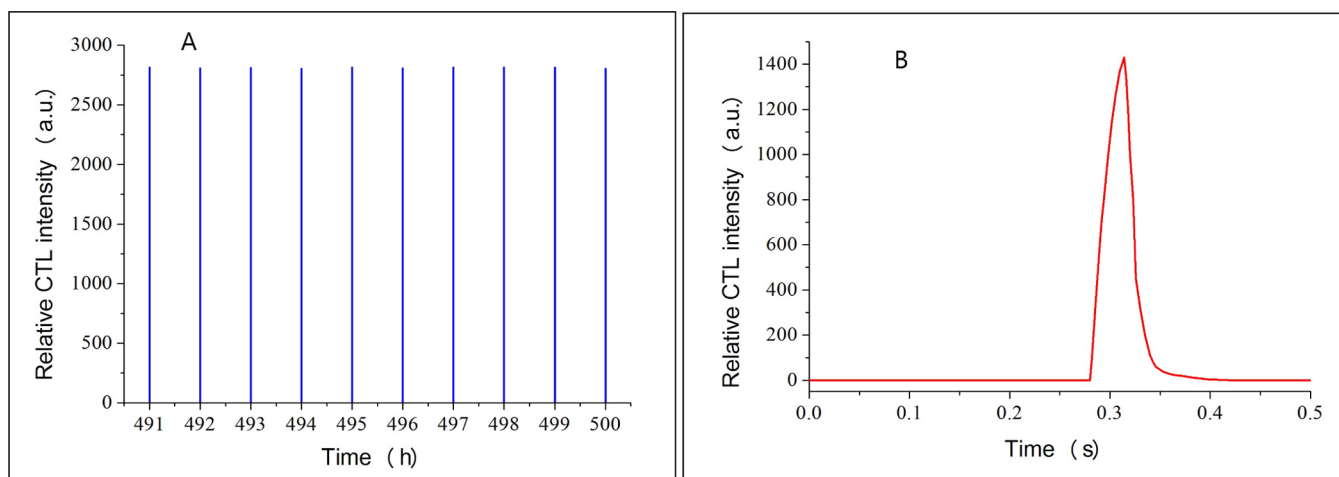


Figure 6. Lifetime test (A) of the sensitive material and response behavior curves (B) of CTL signals.

Pd/ZnNi₃Al₂O₇ had good selectivity for diethyl ether under optimization conditions.

The regression curve of CTL intensity versus diethyl ether concentration was linear in the range of 0.08–75 mg/m³ with a detection limit (3σ) of 0.04 mg/m³ under the optimization conditions. The linear equation is $y = 137.8x + 52.57$ ($R^2 = 0.9990$) in illustration in Figure 7, where y is the CTL intensity, x is the concentration of diethyl ether, and R is the correlation coefficient.

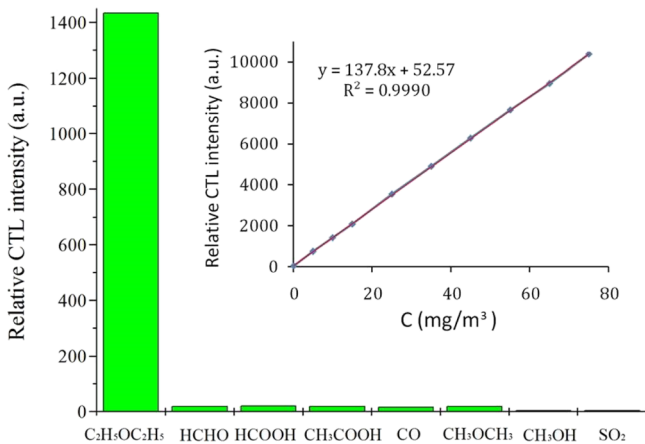
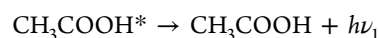
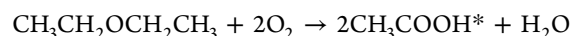


Figure 7. CTL responses of different molecules on nano-Pd/ZnNi₃Al₂O₇ and the linear relationship of CTL intensity versus diethyl ether concentration.

Possible Mechanism. The gaseous analyte was carried onto the surface of the sensitive material by pure air, and the reaction products were analyzed by gas chromatography–mass spectrometry. It is found that when the surface temperature of the sensitive material is about 110 °C, the product will change only when diethyl ether molecules pass through the sensitive material. In other words, not only diethyl ether but also a small amount of acetic acid can be detected. When other molecules, such as formaldehyde, acetaldehyde, formic acid, acetic acid, methanol, ethanol, dimethyl ether, benzene, hydrogen sulfide, sulfur dioxide, carbon monoxide, and other molecules, pass through the sensitive material at about 110 °C, the product does not change. However, not only diethyl ether and acetic acid but also trace carbon dioxide can be detected when diethyl

ether molecules pass through the sensitive material at about 160 °C. At the same time, other molecules, such as formaldehyde, acetic acid, and carbon monoxide, also change when they pass through the sensitive material at about 160 °C. For example, formic acid and carbon dioxide are detected in the product when the formaldehyde molecule passes through the sensitive material, carbon dioxide is detected when the acetic acid molecule passes through, and carbon dioxide is also detected when carbon monoxide passes through.

The possible mechanism is that diethyl ether can be selectively adsorbed and oxidized by the active center on the surface of the sensitive material at about 110 °C to form acetic acid. When the excited acetic acid molecule returns to the ground state, it releases a photon. Other molecules cannot be adsorbed or oxidized by the active center at about 110 °C, so other molecules do not react. When the surface temperature of the sensitive material increases to about 160 °C, diethyl ether can also be adsorbed and oxidized to acetic acid. At the same time, acetic acid molecules that did not leave the sensitive material surface in time can be further oxidized to carbon dioxide. Excited carbon dioxide molecules can also emit a photon when they return to the ground state. In addition, formaldehyde, acetic acid, and carbon monoxide molecules can also be adsorbed and oxidized at about 160 °C and emit photons. The subsequent reactions at high temperature are interference reactions. The reaction mechanism can be expressed by the following formula:



CONCLUSIONS

The present results demonstrated the feasibility to design a highly sensitive diethyl ether gas sensor based on Pd-activated ZnNi₃Al₂O₇ at 109.18 °C, which is a relatively low working temperature in heterogeneous catalytic reaction. The atomic percentage of 0.8–1.3% Pd in nanocomposites was beneficial to the low operating temperature and high selectivity for the CTL of diethyl ether. The sensitivity of the method can be increased by 4.5% after optimizing the experimental conditions by RSM. Nano-Pd/ZnNi₃Al₂O₇ can be a good candidate for fabricating diethyl ether gas sensors.

■ EXPERIMENTAL SECTION

Chemical Reagents and Apparatus. Zinc acetate, nickel chloride, aluminum nitrate, hydrochloric acid, malic acid, ammonia, palladium chloride, and hydrazine hydrate were purchased from Beijing Chemical Regent Co., Ltd. (Beijing, China). Various standard gases of methyl ether, diethyl ether, formaldehyde, acetaldehyde, methanol, ethanol, formic acid, acetic acid, ammonia, benzene, sulfur dioxide, hydrogen sulfide, carbon monoxide, and carbon dioxide in nitrogen were purchased from Beijing Ya-nan Gas Co., Ltd. (Beijing, China). Distilled water was used throughout the whole experiment. The micro area composition and particle morphology of the nano-Pd/ZnNi₃Al₂O₇ were investigated by scanning electron microscopy (SEM, JEOL-IT500) and TEM (JEOL-2100), respectively. The CTL intensities were recorded using an ultraweak luminescence analyzer manufactured at the Biophysics Institute of Chinese Academy of Science (Beijing, China).

Synthesis of Pd/ZnNi₃Al₂O₇. Zinc acetate, nickel chloride, and aluminum nitrate were dissolved in dilute hydrochloric acid. The solution is oscillated by ultrasonication to clear. Malic acid was added into the solution in the stirring state, and the sol was formed by continuously stirring the solution for more than 6 h. The pH value of the solution was adjusted to 5.4 with dilute ammonia water. The solution was stirred for 6 h and aged for 12 h. Then, the gel was prepared by rotating evaporation. After drying and grinding, the gel is placed in a box-type resistance furnace. The temperature is increased to 420 °C at the rate of 4 °C/min and maintained for 5 h. The composite powder of ZnO, NiO, and Al₂O₃ were obtained by natural cooling. Palladium chloride was dissolved in 10% hydrochloric acid aqueous solution, and the composite powder dispersed by ultrasonic waves was added into the solution under stirring. Then, 25% hydrazine hydrate aqueous solution was continuously dripped into the solution under stirring. The solution was subjected to aging, filtering, washing, drying, and calcining at 280 °C in a vacuum oven, successively, to finally get nano-Pd/ZnNi₃Al₂O₇, where the content of Pd can be adjusted by changing the concentration of palladium chloride.

Measurement of Signals of CL on the Solid Catalyst. For the loading of nano-Pd/ZnNi₃Al₂O₇, the adjustment of working temperature, the introduction of the measured gas sample, and the recording of CTL signals, one can refer to our previous work.^{29–35}

Experimental Design for RSM Optimization. According to the single-factor experimental results of analysis wavelength, reaction temperature, and carrier gas velocity, the Box–Behnken central composite experiment was designed, and the CTL experimental conditions of diethyl ether were optimized by RSM at three factors and three levels.

■ AUTHOR INFORMATION

Corresponding Authors

Baining Liu – Biochemical Engineering College, Beijing Union University, Beijing 100023, China; Beijing Key Laboratory of Biomass Waste Resource Utilization, Beijing 100023, China; Email: bainingliu@buu.edu.cn

Kaowen Zhou – Biochemical Engineering College, Beijing Union University, Beijing 100023, China; Beijing Key Laboratory of Biomass Waste Resource Utilization, Beijing 100023, China; orcid.org/0000-0001-6144-3241; Email: zhoukaowen@buu.edu.cn

Authors

Wenjuan Zhang – Biochemical Engineering College, Beijing Union University, Beijing 100023, China; Beijing Key Laboratory of Biomass Waste Resource Utilization, Beijing 100023, China

Fuxiu Yang – Biochemical Engineering College, Beijing Union University, Beijing 100023, China; Beijing Key Laboratory of Biomass Waste Resource Utilization, Beijing 100023, China

Complete contact information is available at:
<https://pubs.acs.org/10.1021/acsomega.1c02098>

Author Contributions

The manuscript was written through contributions of all authors.

Notes

The authors declare no competing financial interest.

■ ACKNOWLEDGMENTS

This work was supported by the Beijing Natural Science Foundation (grant no. 2152013).

■ REFERENCES

- (1) Bai, C.; Liu, N.; Zhang, B. Experimental investigation on the lower flammability limits of diethyl ether/n-pentane/epoxypropane-air mixtures. *J. Loss Prev. Process* **2019**, *57*, 273–279.
- (2) Bai, C.; Wang, Y. Study of the explosion parameters of vapor-liquid diethyl ether/air mixtures. *J. Loss Prev. Process* **2015**, *38*, 139–147.
- (3) Monticelli, F.; Kemmerling, R.; Schulz, K.; Keller, T. Another case of diethyl ether intoxication? A case report focusing on toxicological analysis. *Leg. Med.* **2011**, *13*, 254–258.
- (4) Yang, F.; Gu, C.; Liu, B.; Hou, C.; Zhou, K. Pt-activated Ce₄La₆O₁₇ nanocomposites for formaldehyde and carbon monoxide sensor at low operating temperature. *J. Alloys Compd.* **2019**, *787*, 173–179.
- (5) Wang, Y.; Hu, K.; Zhang, Y.; Ding, X. Dendritic fibrous nano-silica & titania (DFNST) spheres as novel cataluminescence sensing materials for the detection of diethyl ether. *RSC Adv.* **2019**, *9*, 39622–39630.
- (6) Zhen, Y.; Zhang, H.; Fu, F.; Zhang, Y. A cataluminescence sensor based on -MoO₃ nanobelts with low working temperature for the detection of diethyl ether. *J. Mater. Sci. Mater. Electron.* **2019**, *30*, 3722–3728.
- (7) Zhang, L.; He, N.; Shi, W.; Lu, C. A cataluminescence sensor with fast response to diethyl ether based on layered double oxide nanoparticles. *Anal. Bioanal. Chem.* **2016**, *408*, 8787–8793.
- (8) Zhang, L.; Wang, S.; Yuan, Z.; Lu, C. A controllable selective cataluminescence sensor for diethyl ether using mesoporous TiO₂ nanoparticles. *Sens. Actuators, B* **2016**, *230*, 242–249.
- (9) Wang, Q.; Li, B.; Wang, Y.; Shou, Z.; Shi, G. Sensitive and selective cataluminescence-based sensor system for acetone and diethyl ether determination. *Luminescence* **2015**, *30*, 318–324.
- (10) Sha, W.; Gu, P.; Zhang, B.; Zheng, C. A cataluminescence sensor system for diethyl ether based on CdO nanostructure. *Meas. Sci. Technol.* **2014**, *25*, 851028.
- (11) Chen, J.; Cao, X.; Xing, R.; Xu, L.; Liu, Y.; Zeng, J. A Sensor System for Identifying Ether Vapors Based on Extracting Two-stage Cataluminescence Signals. *Acta Chim. Sin.* **2013**, *71*, 1421–1428.
- (12) Liu, J.; Zhang, Y.; Yuan, Y.; Zuo, W. A Nano-Co₃O₄-Based Low Temperature Cataluminescence Sensor for the Detection of Gaseous Ethyl Ether. *Acta Chim. Sin.* **2013**, *71*, 102–106.
- (13) Shi, G.; Sun, B.; Jin, Z.; Liu, J.; Li, M. Synthesis of SiO₂/Fe₃O₄ nanomaterial and its application as cataluminescence gas sensor material for ether. *Sens. Actuators, B* **2012**, *171–172*, 699–704.

- (14) Cao, X.; Wu, W.; Chen, N.; Peng, Y.; Liu, Y. An ether sensor utilizing cataluminescence on nanosized ZnWO₄. *Sens. Actuators, B* **2009**, *137*, 83–87.
- (15) Xiong, S.; Yan, S.; Zhang, L.; Lv, Y. Fluorine functionalized graphitic carbon nitride for cataluminescence sensing of H₂S. *Sens. Actuators, B* **2021**, *339*, 129855.
- (16) Hu, J.; Zhang, L.; Song, H.; Su, Y.; Lv, Y. Ozone-induced ratiometric cataluminescence for aromatic compounds discrimination based on Eu,Tb co-doped MgO. *Sens. Actuators, B* **2021**, *327*, 128939.
- (17) Zhong, Y.; Shi, Z.; Wen, T.; Xiao, X.; Li, G.; Hu, Y. Cataluminescence strategy for rapid identification of sunscreen cosmetics based on its characteristic composition served as catalyst. *Sens. Actuators, B* **2020**, *323*, 128697.
- (18) Zhang, R. K.; Wang, J. X.; Cao, H. High-performance cataluminescence sensor based on nanosized V₂O₅ for 2-butanone detection. *Molecules* **2020**, *25*, 25153552.
- (19) Li, L.; Yang, Y.; Deng, D.; Song, H.; Lv, Y. Photocatalysis enhanced cataluminescence gas sensor for carbon monoxide based on perylenetetracarboxylic diimide. *Sens. Actuators, B* **2020**, *315*, 128080.
- (20) Yu, K.; Hu, J.; Li, X.; Zhang, L.; Lv, Y. Camellia-like NiO: A novel cataluminescence sensing material for H₂S. *Sens. Actuators, B* **2019**, *288*, 243–250.
- (21) Shi, G.; He, Y.; Zhang, Y.; Yin, B.; Ali, F. Detection and determination of harmful gases in confined spaces for the Internet of Things based on cataluminescence sensor. *Sens. Actuators, B* **2019**, *296*, 126686.
- (22) Meng, F.; Lu, Z.; Zhang, R.; Li, G. Cataluminescence sensor for highly sensitive and selective detection of iso-butanol. *Talanta* **2019**, *194*, 910–918.
- (23) Li, L.; Wei, C.; Song, H.; Yang, Y.; Xue, Y.; Deng, D.; Lv, Y. Cataluminescence Coupled with Photoassisted Technology: A Highly Efficient Metal-Free Gas Sensor for Carbon Monoxide. *Anal. Chem.* **2019**, *91*, 13158–13164.
- (24) Kato, S.; Ito, Y.; Ikuta, Y.; Morikawa, A.; Suda, A.; Tanabe, T. Demonstrating the Potential of Chemiluminescence as a Tool to Characterize Heterogeneous Catalysis Using CO Oxidation on Copper-Based Catalysts as an Example. *ChemCatChem* **2019**, *11*, 2423–2426.
- (25) Zeng, N.; Long, Z.; Wang, Y.; Sun, J.; Ouyang, J.; Na, N. An Acetone Sensor Based on Plasma-Assisted Cataluminescence and Mechanism Studies by Online Ionizations. *Anal. Chem.* **2019**, *91*, 15763–15768.
- (26) Li, L.; Deng, D.; Huang, S.; Song, H.; Xu, K.; Zhang, L.; Lv, Y. UV-Assisted Cataluminescent Sensor for Carbon Monoxide Based on Oxygen-Functionalized g-C₃N₄ Nanomaterials. *Anal. Chem.* **2018**, *90*, 9598–9605.
- (27) Zhang, R.; Wang, Y.; Zhang, Z.; Cao, J. Highly Sensitive Acetone Gas Sensor Based on g-C₃N₄ Decorated MgFe₂O₄ Porous Microspheres Composites. *Sensors* **2018**, *18*, 22117.
- (28) Shi, G.; He, Y.; Luo, Q.; Li, B.; Zhang, C. Portable device for acetone detection based on cataluminescence sensor utilizing wireless communication technique. *Sens. Actuators, B* **2018**, *257*, 451–459.
- (29) Zhou, K.; Xu, J.; Gu, C.; Liu, B.; Peng, Z. Identification and determination of formaldehyde, benzene and ammonia in air based on cross sensitivity of cataluminescence on single catalyst. *Sens. Actuators, B* **2017**, *246*, 703–709.
- (30) Zhou, K.; Xu, J.; Gu, C.; Hou, C.; Ren, H. Simultaneous determination of trimethylamine, formaldehyde and benzene via the cataluminescence of In₃LaTi₂O₁₀ nanoparticles. *Microchim. Acta* **2017**, *184*, 2047–2053.
- (31) Fan, H.; Cheng, Y.; Gu, C.; Zhou, K. A novel gas sensor of formaldehyde and ammonia based on cross sensitivity of cataluminescence on nano-Ti₃SnLa₂O₁₁. *Sens. Actuators, B* **2016**, *223*, 921–926.
- (32) Yang, F.; Zhang, W.; Zhao, Y.; Ji, Y.; Liu, B.; Zhou, K. Optimization of Working Conditions by Response Surface Methodology of Sulfur Dioxide Gas Sensors Based on Au/CoO-2La₂WO₆ Nanoparticles. *Chemistryselect* **2020**, *5*, 11145–11151.
- (33) Zhang, W.; Yang, F.; Xu, J.; Gu, C.; Zhou, K. Sensitive Carbon Monoxide Gas Sensor Based on Chemiluminescence on Nano-Au/Nd₂O₃-Ca₃Nd₂O₆: Working Condition Optimization by Response Surface Methodology. *ACS Omega* **2020**, *5*, 20034–20041.
- (34) Zhang, W.; Yang, F.; Wang, H.; Gu, C.; Lu, Y.; Zhou, K. High-performance hydrogen sulfide gas sensor based on Pd/Fe₂O₃-Zr₄MnO₁₀: working conditions optimization by response surface methodology. *J. Iran. Chem. Soc.* **2020**, *17*, 3401–3410.
- (35) Yang, F.; Zhang, W.; Wang, H.; Gu, C.; Lu, Y.; Zhou, K. Determination of formaldehyde using a novel Pt-doped nano-sized sensitive material: Operating conditions optimization by response surface method. *Anal. Chim. Acta* **2020**, *1132*, 47–54.
- (36) Karimi-Maleh, H.; Yola, M. L.; Atar, N.; Orooji, Y.; Karimi, F.; Senthil Kumar, P.; Rouhi, J.; Baghayeri, M. A novel detection method for organophosphorus insecticide fenamiphos: Molecularly imprinted electrochemical sensor based on core-shell Co₃O₄ @ MOF-74 nanocomposite. *J. Colloid Interface Sci.* **2021**, *592*, 174–185.
- (37) Karimi-Maleh, H.; Alizadeh, M.; Orooji, Y.; Karimi, F.; Baghayeri, M.; Rouhi, J.; Tajik, S.; Beitollahi, H.; Agarwal, S.; Gupta, V. K.; Rajendran, S.; Rostamnia, S.; Fu, L.; Saberi-Movahed, F.; Malekmohammadi, S. Guanine-based DNA biosensor amplified with Pt/SWCNTs nanocomposite as analytical tool for nanomolar determination of daunorubicin as an anticancer drug: a docking/experimental investigation. *Ind. Eng. Chem. Res.* **2021**, *60*, 816–823.
- (38) Shi, Y.; Wang, J.; Zhou, R. Pt-support interaction and nanoparticle size effect in Pt/CeO₂-TiO₂ catalysts for low temperature VOCs removal. *Chemosphere* **2021**, *265*, 129127.
- (39) Karimi-Maleh, H.; Kumar, B. G.; Rajendran, S.; Qin, J.; Vadivel, S.; Durgalakshmi, D.; Gracia, F.; Soto-Moscoso, M.; Orooji, Y.; Karimi, F. Tuning of metal oxides photocatalytic performance using Ag nanoparticles integration. *J. Mol. Liq.* **2020**, *314*, 113588.
- (40) Tahernejad-Javazmi, F.; Shabani-Nooshabadi, M.; Karimi-Maleh, H. Analysis of glutathione in the presence of acetaminophen and tyrosine via an amplified electrode with MgO/SWCNTs as a sensor in the hemolyzed erythrocyte. *Talanta* **2018**, *176*, 208–213.
- (41) Alavi-Tabari, S. A. R.; Khalilzadeh, M. A.; Karimi-Maleh, H. Simultaneous determination of doxorubicin and dasatinib as two breast anticancer drugs uses an amplified sensor with ionic liquid and ZnO nanoparticle. *J. Electroanal. Chem.* **2018**, *811*, 84–88.
- (42) Du, X.; Dong, F.; Tang, Z.; Zhang, J. The synthesis of hollow In₂O₃ @ Pd-Co₃O₄ core/shell nanofibers with ultra-thin shell for the low-temperature CO oxidation reaction. *Appl. Surf. Sci.* **2020**, *505*, 144471.
- (43) He, Y.; Luan, C.; Fang, Y.; Feng, X.; Peng, X.; Yang, G.; Tsubaki, N. Low-temperature direct conversion of methane to methanol over carbon materials supported Pd-Au nanoparticles. *Catal. Today* **2020**, *339*, 48–53.
- (44) Marcinkowski, M. D.; Yuk, S. F.; Doudin, N.; Smith, R. S.; Nguyen, M.-T.; Kay, B. D.; Glezakou, V.-A.; Rousseau, R.; Dohnálek, Z. Low-Temperature Oxidation of Methanol to Formaldehyde on a Model Single-Atom Catalyst: Pd Atoms on Fe₃O₄(001). *ACS Catal.* **2019**, *9*, 10977–10982.
- (45) Du, X.; Han, W.; Tang, Z.; Zhang, J. Controlled synthesis of Pd/CoOx-InOx nanofibers for low-temperature CO oxidation reaction. *New J. Chem.* **2019**, *43*, 14872–14882.
- (46) Khder, A. E. R. S.; Altass, H. M.; Orif, M. I.; Ashour, S. S.; Almazroai, L. S. Preparation and characterization of highly active Pd nanoparticles supported Mn₃O₄ catalyst for low-temperature CO oxidation. *Mater. Res. Bull.* **2019**, *113*, 215–222.
- (47) Zhou, K.; Zhou, Y.; Li, W.; Zhang, Y. Nanocomposites for monitoring ether. CN 201310199379.9 A, 2015.
- (48) Pinto, D.; Vieira, E. F.; Peixoto, A. F.; Freire, C.; Freitas, V.; Costa, P.; Delerue-Matos, C.; Rodrigues, F. Optimizing the extraction of phenolic antioxidants from chestnut shells by subcritical water extraction using response surface methodology. *Food Chem.* **2021**, *334*, 127521.
- (49) Singh, T. S.; Rajak, U.; Samuel, O. D.; Chaurasiya, P. K.; Natarajan, K.; Verma, T. N.; Nashine, P. Optimization of performance and emission parameters of direct injection diesel engine fuelled with

microalgae *Spirulina* (L.) - Response surface methodology and full factorial method approach. *Fuel* **2021**, *285*, 119103.

(50) Keramat, E.; Hashemi, B. Modelling and optimizing the liquid phase sintering of alumina/CaO-SiO₂-Al₂O₃ ceramics using response surface methodology. *Ceram. Int.* **2021**, *47*, 3159–3172.

(51) Preskar, M.; Videc, D.; Vrečer, F.; Gašperlin, M. Investigation of design space for freeze-drying injectable ibuprofen using response surface methodology. *Acta Pharm.* **2021**, *71*, 81–98.